Marine Chemistry 118 (2010) 99–107

Contents lists available at ScienceDirect

Marine Chemistry

journal homepage: www.elsevier.com/locate/marchem

Pore-water geochemistry of two contrasting brine-charged seep sites in the northern Gulf of Mexico continental slope

Xinping Hu [a,*], Wei-Jun Cai [a], Yongchen Wang [a], Shangde Luo [b], Xianghui Guo [a,c]

[a] Department of Marine Sciences, the University of Georgia, Athens, GA 30602, USA
[b] Department of Earth Sciences, National Chung-Kung University, Tainan 701, Taiwan
[c] State Key Laboratory of Marine Environmental Science, Xiamen University, Xiamen, Fujian, China

ARTICLE INFO

Article history:
Received 4 June 2009
Received in revised form 4 November 2009
Accepted 24 November 2009
Available online 1 December 2009

Keywords:
Brines
Stable isotopes
Inorganic carbon
Pore water
Gulf of Mexico

ABSTRACT

Two brine-charged sites (GB425 and GC233) at the northern Gulf of Mexico (GOM) continental slope were studied for their pore-water advective flow rates and stable carbon isotope geochemistry. Using chloride as a conservative tracer, a pore-water diffusion–advection model suggests that advection dominates pore-water flow in the upper 17 cm sediments at both sites. Moreover, modeled results indicate that there is a downward pore-water flow in GB425 and an upward one in GC233, presumably caused by nearby brine-seep activities. Profiles of pore-water solutes (dissolved inorganic carbon, or DIC, sulfate, and ammonium) can be largely explained by conservative mixing between bottom water and underlying brines, which contain dissolved species that are produced at or below a subsurface reaction front, where sulfate reduction coupled with organic carbon oxidation occurs. Stable carbon isotope data indicate that organic carbon being remineralized has a similar $\delta^{13}C$ value (−40 to −60‰) as that of thermogenic and biogenic methane found in this area. However, without further evidence, the exact carbon source and reaction pathway remain unclear.

1. Introduction

Natural, gas-hydrate-associated cold seeps are a common geological feature widely observed in marine continental margin sediments (Kvenvolden, 1988; Milkov, 2004). Unlike common marine sediments that receive organic carbon deposition almost exclusively from surface water production, organic carbon sources that drive benthic microbial respiration in cold seep environments come mostly from subsurface (e.g., Joye et al., 2009). For example, active venting of microbial or thermogenic hydrocarbons and their metabolic products, which are more depleted in ^{13}C than organic carbon of planktonic origin, is often observed in seep environments (e.g., Joye et al., 2009; Sassen et al., 2004).

Cold seeps in the northern Gulf of Mexico (GOM) continental margin, unlike many other seep environments around the world, are caused by extensive salt diapir formation (Aharon et al., 1992). These salt diapirs are formed through sediment compaction following deposition of terrigenous sediments on top of ancient (Jurassic) salt deposits, because sediment compaction results in denser overlying sediment layer so that its weight drives upward salt flow over time (Joye et al., 2005, and references therein; MacDonald et al., 1990, and references therein). Brines are formed by dissolving subsurface salt deposits in many areas of the northern GOM slope, and brine seeps may be an important conduit through which deeply-buried hydrocarbons are delivered to shallow sediment depths and even the water column (Joye et al., 2005; Lapham et al., 2008). Previous studies have explored geochemical properties of brine-water "lakes" (i.e., a pool of dense brine that is in contact with overlying seawater and lying in a seafloor depression) via geochemical analyses (Aharon et al., 1992; Joye et al., 2005; Joye et al., 2009). Meanwhile, both direct measurements and pore-water modeling are used to estimate brine flow rates in various seep environments (Lapham et al., 2008; Reitz et al., 2007; Solomon et al., 2008; Tryon and Brown, 2004), given that the direction and rate of this flow have important implications in understanding the export of subsurface hydrocarbons to overlying water column. However, we still know little about fine-scale pore-water dynamics in surface sediments under the influence of brines. In the literature, conservative mixing between seawater and deep brine has been observed in sediments from both the Florida escarpment and northern GOM continental slope (Chanton et al., 1991; Chanton et al., 1993; Lapham et al., 2008), it is thus of interest to examine whether such mixing can be observed in other GOM sediments. This work will serve as an addition to current knowledge on pore-water flow in brine-charged sediments.

As a part of the broader Shelf Slope Experimental Taphonomy Initiative (SSETI, cf. Parsons et al., 1997) study, we examined pore-water geochemistry in two GOM brine-charged sites (GB425 and GC233) to estimate pore-water flow rates. At the same time, using

* Corresponding author. Tel.: +1 706 583 0436; fax: +1 706 542 5888.
E-mail address: xhu@uga.edu (X. Hu).

0304-4203/$ – see front matter © 2009 Elsevier B.V. All rights reserved.
doi:10.1016/j.marchem.2009.11.006

stable carbon isotope technique, we also explored possible carbon sources that contribute to the dissolved inorganic carbon (DIC) pool in pore waters.

2. Materials and methods

2.1. Site descriptions

Sediment cores were collected in September, 2006 using the *R/V Seward Johnson* and onboard the submersible *Johnson Sea Link* as our operating platforms. Two sites near brine seeps in the Garden Bank and Green Canyon areas were sampled. Surface sediments at site GB425 (27°33.6′ N, 92°32.3′ W; water depth, 570 m) were free of visible microbial mats and a mud volcano was in the vicinity (estimated distance ~50–100 m). Site GC233 (27°43.4′ N, 91°16.9′ W; water depth, 650 m) was located in a microbial mat-covered area <5 m away from a ring of mussels, the latter surrounding a brine pool (K. Parsons-Hubbard, pers. comm.).

2.2. Sample collection and processing

Push cores were collected using 30 cm-long butyl core tubes (i.d.= 8 cm) equipped with one-way check valves at the top of these core tubes. This design facilitates the escape of entrapped water in the upper core tube as the core tube is slowly inserted into sediment. 4–5 whole cores with lengths ranging ~18–25 cm were collected at each site. Immediately after the cores arrived on board, they were sealed at the bottom using rubber stoppers and then transferred to a shipboard cold room, which was maintained close to bottom water temperature (~7–8 °C). Visual inspection of these cores did not observe carbonate crusts or macrofauna. Core sectioning was carried out using a hydraulic extruder (Cai et al., 2006; Joye et al., 2004). The depth intervals sampled were 0–1, 1–2, 2–3, 3–5, 5–7, 7–10, 10–14, and 14–17 cm. Within 2 h of core recovery, all sectioned core intervals were compressed under N_2 pressure using the same gas-actuated Reeburgh-type core squeezers as described in Joye et al. (2004). Pore-water samples were received using 50-ml disposable plastic syringes and then filtered through 0.45-μm nylon disc filters into appropriate storage vessels for further analyses. Total alkalinity (TA) and dissolved inorganic carbon (DIC and $\delta^{13}C$) samples were preserved using saturated $HgCl_2$ solution (0.02 ml for every 5 ml of sample). Sulfate samples were acidified using concentrated HNO_3 (0.1 ml for every 0.5 ml of sample). Sulfide samples were preserved using saturated zinc acetate (0.5 ml for every 1 ml of sample, Joye et al., 2004). Ammonium samples were analyzed immediately after pore-water collection. All other pore-water samples were kept refrigerated at 4 °C in the dark until analysis.

2.3. Pore-water analytical methods

TA was determined by Gran titration referenced to a certified reference material (CRM) from A. Dickson (Scripps). DIC was determined using an infrared CO_2 detector after acid extraction (Cai and Wang, 1998). The same CRM was also used as a standard in DIC analysis. $\delta^{13}C$ of DIC ($\delta^{13}C_{DIC}$) was measured at UC Davis Stable Isotope Facility and reported relative to VPDB. Pore-water total halides were determined by $AgNO_3$ titration with potassium chromate and potassium dichromate as the end-point indicator (Grasshoff et al., 1999). This measurement will be referred to as chloride concentration because Br^- and I^- concentrations together rarely exceed 1 mM in both deep sea sediments (Gieskes and Mahn, 2007) and sediments that contain gas hydrates (e.g., Muramatsu et al., 2007). Sulfate concentration was determined using ion chromatography (Grasshoff et al., 1999). NaCl solution and IAPSO standard seawater were used as standards in $AgNO_3$ titration and IC analysis, respectively (Grasshoff et al., 1999). Calcium concentration was determined using EGTA titration (Grasshoff et al., 1999). Total alkaline earth element concentration (Mg, Ca, Sr, and Ba) was determined using spectrophotometric EDTA titration (Grasshoff et al., 1999). Magnesium concentration was calculated by subtracting contributions from both calcium and strontium (barium is negligible when sulfate is present), the latter was estimated using Sr/Cl ratio in standard seawater, given relatively small Sr enrichment in brine waters (Schijf, 2007) and low overall strontium concentrations compared to calcium and magnesium. EGTA and EDTA titrants were standardized using standard solutions made from $CaCO_3$ and Mg metal following the procedures in Grasshoff et al. (1999). Sulfide concentration was determined using the colorimetric method of Cline (1969). Ammonium concentration was determined using the indophenol colorimetric method as described in Pai et al. (2001).

Uncertainties of our analyses were: TA (±0.1%), DIC (±0.1%), Ca^{2+} (±0.2%), Mg^{2+} (±0.2%), $\delta^{13}C_{DIC}$ (±0.2‰), sulfate (±1%), sulfide (±2%), ammonia (2%), and Cl^- (±0.2%).

3. Results

3.1. General trends of pore-water profiles

Pore-water chloride concentrations increased with depth at both sites and reached maximum values of 804.6 mM (GB425) and 762.4 mM (GC233) at the core bottom (15.5 cm, i.e., the 14–17 cm interval, Table 1 and Fig. 1). TA and DIC concentrations also increased sharply by 4–6 times of the bottom water values at the core bottom. In addition, TA and DIC values were linearly correlated with each other (slope = 1.17, r^2 = 1.00). Sulfate concentrations decreased with depth at both sites but sulfate was not completely depleted at the core bottom at either site (minimum concentrations were 11–12 mM). In comparison, in the upper 10 cm of GB425 sediments, sulfide was nearly undetectable, but a fast increase to ~1 mM was observed at the core bottom (10–17 cm); GC233 had a monotonic increase in sulfide and its concentration reached 6.8 mM at the core bottom. Ammonium concentration in GB425 showed a mid-depth maximum (0.17 mM) at 8.5 cm and decreased to 0.06 mM at the core bottom. In GC233, ammonium exhibited a monotonic increase from zero in the bottom water to 0.67 mM at core bottom. We cannot explain the apparent ammonium concentration discontinuity in GB425. Previously, our 2001 results (Cai, unpublished data) at a similar GB425 sediment had a maximum ammonium concentration of ~0.29 mM at the 7–10 cm depth interval, although the core we took then was much shorter (10 cm). The two deep data points in GB425 will be excluded for pore-water modeling purposes (Section 4.1). Nevertheless, the fact that lower ammonium concentrations in GB425 pore waters than those of GC233 appears to be consistent with ammonium concentration difference observed directly from the two brine seeps (~7.6 at GB425 vs. ~10.8 mM at GC233, Joye et al., 2005).

Changes in Ca^{2+} and Mg^{2+} profiles were relatively subtle when compared with their bottom water background values. At GB425, Ca^{2+} showed a general increasing trend although with relatively large variations; Mg^{2+} exhibited an initial increase and then a decrease to a concentration of 52.5 mM at the core bottom, which was lower than the bottom water value of 54.7 mM. At GC233, Ca^{2+} had an initial increase in the top 3 cm of sediments, and then decreased to 10.0 mM at the core bottom; Mg^{2+} showed a mid-depth minimum at 4 cm depth (51.7 mM) and then increased to 52.4 mM at the core bottom. Chloride-normalized Ca^{2+} and Mg^{2+} profiles reduced much of the data scattering and both showed decreasing trends with depth (panels E and J, Fig. 1).

3.2. $\delta^{13}C_{DIC}$

In GB425, pore-water $\delta^{13}C_{DIC}$ showed small variations in the upper 4 cm of sediments, and then decreased almost linearly, reaching ~−40‰ at the core bottom. $\delta^{13}C_{DIC}$ in GC233 exhibited a sharper

Table 1
Sediment porosity and pore-water solute chemistry.

Site	Depth (cm)	Porosity[b] (%)	Cl^- (mM)	DIC (mM)	$\delta^{13}C_{DIC}$ (‰VPDB)	TA (mM)	NH_4^+ (mM)	Ca^{2+} (mM)	Mg^{2+} (mM)	SO_4^{2-} (mM)	H_2S (mM)
GB425	BW[a]	96.6	558.4	2.253	0.1	2.489	0.000	10.38	54.71	28.7	0.003
	0–1	95.3	611.6	2.588	−2.0	2.875	0.015	11.48	59.18	29.7	0.004
	1–2	92.7	627.4	2.901	−3.7	3.600	0.044	12.00	59.42	28.8	0.004
	2–3	92.1	606.9	3.202	−1.5	3.728	0.068	11.36	55.98	29.3	0.005
	3–5	87.9	629.9	3.787	−3.9	4.618	0.061	11.56	57.31	28.8	0.004
	5–7	87.6	671.0	4.507	−9.1	5.398	0.100	12.11	58.60	28.4	0.004
	7–10	75.8	635.3	5.925	−16.1	6.401	0.172	11.17	52.10	26.6	0.000
	10–14	73.8	712.5	8.228	−33.5	9.126	0.079	11.52	52.77	21.5	1.115
	14–17	73.4	804.6	11.087	−40.2	13.316	0.057	12.36	52.52	12.4	1.135
GC233	BW[a]	88.3	561.7	2.267	−0.3	2.513	0.000	10.42	54.71	28.5	0.003
	0–1	85.6	631.9	4.019	−24.8	4.472	0.320	11.87	55.83	29.4	0.009
	1–2	80.2	632.6	4.983	−29.2	5.407	0.434	11.90	54.13	25.3	0.168
	2–3	74.6	660.3	6.362	−37.3	7.073	0.476	12.19	53.09	23.0	0.614
	3–5	70.3	685.7	8.821	−44.9	9.964	0.521	11.64	51.67	22.2	1.199
	5–7	69.0	709.4	10.751	−49.1	11.974	0.543	11.13	52.02	20.5	2.298
	7–10	66.8	714.3	11.977	−49.4	13.712	0.626	10.75	52.29	16.8	2.230
	10–14	66.0	745.9	14.371	−49.6	16.848	0.645	10.53	51.92	14.7	5.288
	14–17	68.0	762.4	14.761	−47.1	16.741	0.670	9.99	52.36	11.3	6.789

[a] BW denotes bottom water.
[b] Porosity at sediment–water interface was calculated using the fitted exponential decay functions (Berner, 1980).

decrease with depth and reached ~−50‰ at the core bottom. Overall, DIC and $\delta^{13}C$ profiles mirrored each other at both sites (Fig. 1).

Linear regression of DIC concentrations multiplied by $\delta^{13}C_{DIC}$ (i.e., $DIC\times\delta^{13}C$) vs. DIC has been used previously to examine stable isotopic composition of DIC added ($\delta^{13}C_{added}$ = regression slope) into the pore-water DIC pool, through both reaction and mixing. $\delta^{13}C_{added}$ is defined as the isotopic value of the bulk DIC being added to the initial pore-water DIC background since the burial of bottom water (e.g., Hu and Burdige, 2007; Martin et al., 2000). This approach yields essentially the same value as that obtained from regression of $\delta^{13}C$ *vs.* DIC^{-1}, where the regression intercept is $\delta^{13}C_{added}$ (Hu, 2007; LaZerte, 1981). Using the linear regression of $DIC\times\delta^{13}C$ vs. DIC,

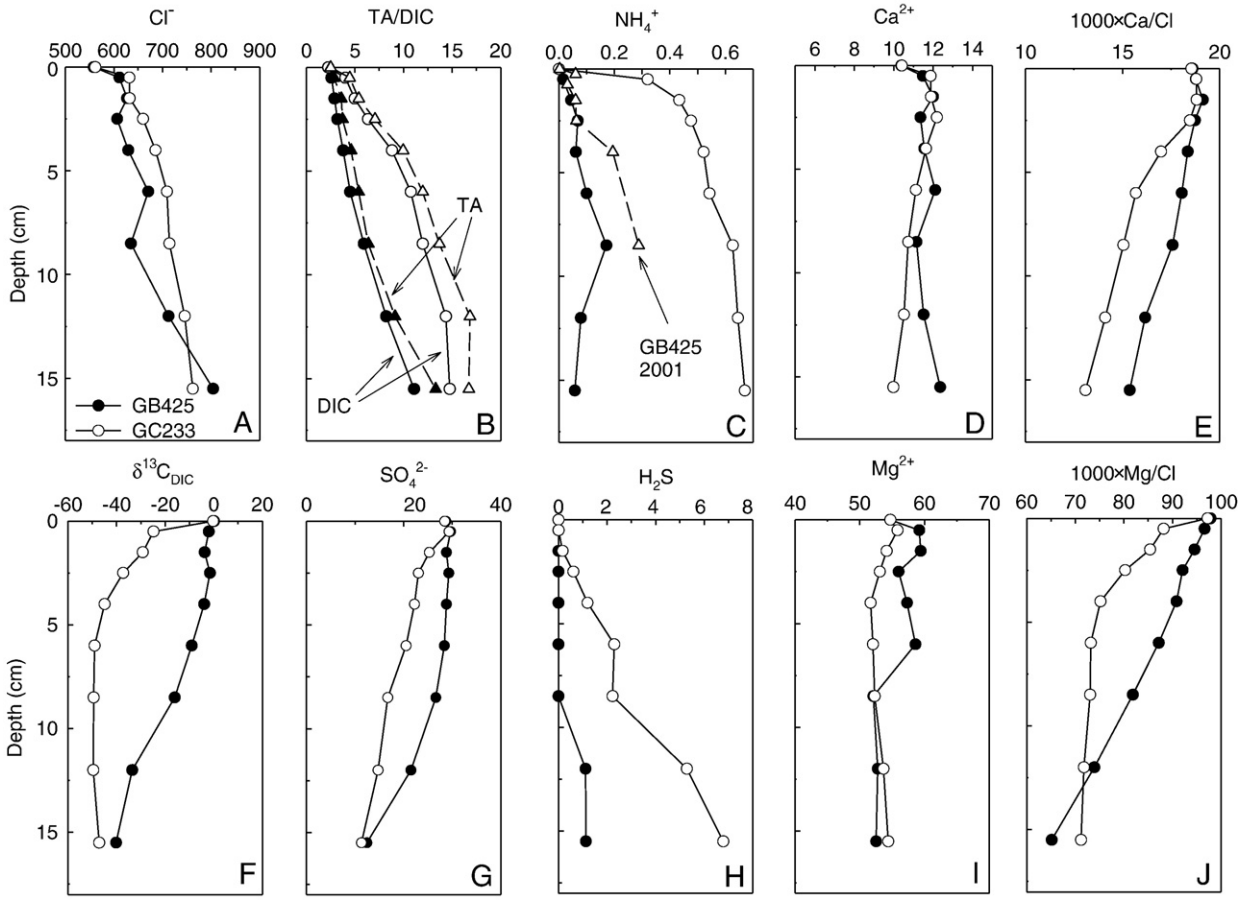

Fig. 1. Pore-water profiles of chloride, $\delta^{13}C_{DIC}$, TA/DIC, sulfate, ammonium, sulfide, calcium, and magnesium. Unit for all solutes is mM, and unit for isotopic value ($\delta^{13}C$) is per mil (‰ VPDB). The two panels at far right (E and J) show chloride-normalized calcium and magnesium profiles. Filled symbols represent GB425 data, and open symbols represent GC233 data. Note triangles are used to illustrate TA profiles in panel B. In panel C, ammonium profile from our 2001 trip (Cai, unpublished data) is also plotted along.

calculated $\delta^{13}C_{added}$ values at GB425 and GC233 sites are -53.4 ± 4.1‰ and -58.6 ± 2.1‰, respectively (Fig. 2).

4. Discussion

4.1. Diffusion–advection model and pore-water flow rates

Conservative solutes (chloride or its expression as salinity, and lithium) have been previously used in modeling pore-water transport in brine-charged sediments (Lapham et al., 2008; Reitz et al., 2007; Ruppel et al., 2005), due to the fact that these solutes undergo little diagenetic changes. Because chloride concentrations exhibited conspicuous enrichment at depth in both GB425 and GC233, we can use chloride as a tracer to examine pore-water advection using Eq. (1) and assuming steady-state conditions (Lapham et al., 2008):

$$\frac{d}{dx}\left(\varphi D_s \frac{dC}{dx}\right) - v\varphi\frac{dC}{dx} = 0 \quad (1)$$

where sediment porosity (φ) is an exponential decay function of sediment depth (Berner, 1980), D_s is whole sediment diffusivity which can be expressed as $D_0/(1-\ln(\varphi^2))$ (e.g., Burdige, 2006). D_0 is the diffusion coefficient in free solution and its value is a function of salinity, temperature and pressure (Boudreau, 1997), and v is the sum of pore-water advection caused by both brine flow and burial of pore water due to sedimentation (Lapham et al., 2008). Furthermore, according to mass balance, $v\varphi$ (or as a single variable V) is a constant value despite the fact that each term individually varies with depth (Burdige, 2006); thus we will use V as a single unknown in our following calculations.

In solving Eq. (1), we may consider two types of boundary conditions (Neumann and Dirichlet vs. Dirichlet boundary conditions, Holzbecher, 2007). First, we take a combination of Neumann and Dirichlet conditions, i.e., a zero concentration gradient at infinite depth ($dC/dx|_{x=\infty}=0$, Neumann) and a known upper boundary condition (C_0, Dirichlet), thus both V and C_∞ are fitting parameters. Second, for the Dirichlet conditions, we take both the upper and lower boundary concentrations as known, thus V is the only fitting parameter.

Bottom water samples were obtained using a Niskin bottle which was attached to the submersible at about 1 m above the seafloor. Thus, bottom water samples are likely not affected by mixing with pore waters due to the existence of benthic boundary layer (e.g., Reimers et al., 2000) and possible horizontal brine flow induced stratification at the sediment surface (especially for GC233). Therefore in the pore-water model we take pore-water concentration at 0.5 cm sediment depth as the upper boundary condition.

In applying the Dirichlet boundary conditions, the upper boundary condition remains the same (i.e., $C_{x=0.5}=C_0$). However, the lower boundary condition needs to be further examined. A number of studies reported brine-water concentrations found at both brine seeps and adjacent sediment pore waters in the Gulf of Mexico. At the same time, maximum chloride concentrations were also observed to occur at different depths (Table 2). It is clear that both brine seep and associated sediment pore waters have highly variable chloride concentrations. These variabilities are likely caused by either the differences in original brine concentrations from their respective sources (Reitz et al., 2007) or the distance between observed sediments and active brine seeps, i.e., the chloride gradient becomes smaller when sampling site moves further away from a brine seep (e.g., Castellini et al., 2006). Furthermore, the lengths of sediment cores often times limit our ability in predicting the concentration of the actual brine coming from underneath. In this study, we choose three different lower boundary conditions (see below) based on comparisons of both site locations (GB425 and GC233) relative to those in the literature and depth ranges which are comparable to the short cores sampled in this work. Thus decisions on lower boundary condition are arbitrary but should be reasonable in reflecting upper sediment pore-water dynamics.

In the following modeling practice using Dirichlet boundary conditions, we apply three sets of lower boundary conditions, (1). $C_{x=15.5\,cm}=C_m$, (2). $C_{x=100\,cm}=C_{SBJ}$, (3). $C_{x=100\,cm}=C_{LL}$. Here C_m is the measured chloride concentration at 15.5 cm; C_{SBJ} is brine-water chloride concentration (i.e., 2082 and 2073 mM for GB425 and GC233, respectively) from Joye et al. (2005); and C_{LL} is the measured brine-water chloride concentration (i.e., 4500 mM) from Lapham et al. (2008). For both cases (2) and (3), we arbitrarily assume that 100 cm is the lower boundary depth (e.g., Lapham et al, 2008). In solving the model, we use two different MatLab® routines (ode45 and bvp4c) to find least square fits to the observed pore-water chloride profiles for these two types of boundary conditions. Based on these least square fits we can then obtain either an optimal pair of V and C_∞ values (for the Neumman and Dirichlet boundary conditions) or an optimal V value (for the Dirichlet boundary conditions) (Fig. 3 and Table 3).

The pore-water chloride model for GB425 appears relatively insensitive to either the choice of modeling approaches (i.e., type of boundary conditions) or the deep, brine-water chloride concentrations, due to relatively scattered data points. Modeled pore-water advection rates at the sediment–water interface ($v_0=V/\varphi_0$, and φ_0 is calculated porosity at sediment–water interface using the exponential decay function as discussed above) range between ~30 cm yr^{-1} downward advection and 6 cm yr^{-1} upward advection. The ^{210}Pb-based sedimentation rate in GOM continental slope area of 1.5–3.0×10^{-2} cm yr^{-1} is almost negligible compared to the calculated advection rates (Hu, unpublished data; also see Yeager et al., 2004). The GC233 model also produces a range of V values, although the model runs based on both the Neumann and Dirichlet and the Dirichlet conditions (1) appear to fit the observed pore-water profiles the best (Table 3 and Fig. 3). Furthermore, the high brine-water chloride concentrations from both Joye et al. (2005) and Lapham et al.

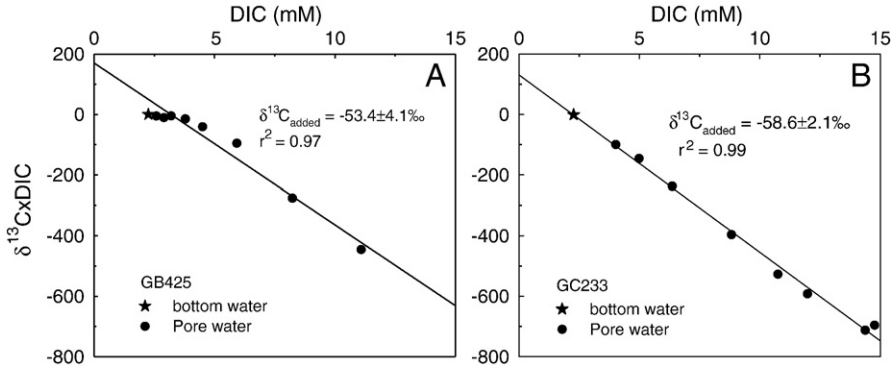

Fig. 2. $\delta^{13}C_{added}$ calculated using the linear regression of $\delta^{13}C\times DIC$ vs. DIC in (A) GB425 and (B) GC233 sediments.

Table 2
Brine-water chloride concentration observed in the Gulf of Mexico continental slope.

Site[a]	Cl (mM)	Depth (cm)	Reference
Brine seeps			
GB425	2082	–	Joye et al. (2005)
GC233	2073	–	Joye et al. (2005)
GK	2058–4571	–	Aharon et al. (1992)
Pore waters			
GC and MC709	2200–4460	8–38	Lapham et al. (2008)
KC151	934	37,030	Kastner et al. (2008)
AT13/14	971	100	Kastner et al. (2008)
GB425	2724	202	Castellini et al. (2006)
MC852/853	2606	133	Castellini et al. (2006)
GC185	665	9	Arvidson et al. (2004)
GC234	738	24	Arvidson et al. (2004)
GB425	1698	20	Arvidson et al. (2004)
GC233	841	10	Arvidson et al. (2004)
GB425	805	15.5	This study
GC233	762	15.5	This study

[a] GK, MC, KC, and AT are abbreviations for Green Knoll, Mississippi Canyon, Keathley Canyon, and Atwater Valley areas, respectively.

(2008) do not appear to produce satisfactory fits to our chloride profiles.

The *V* values calculated from fitting the chloride profiles can be used to simulate pore-water sulfate, DIC, and ammonium profiles under a mixing scenario. We assume that any deviation from a mixing scheme can be attributed to reactions. First, a comparison of these boundary conditions suggests that the *V* values for both sites obtained using the Dirichlet boundary conditions (1) (i.e., -29 cm yr^{-1} for GB425 and 27 cm yr^{-1} for GC233; here the negative value indicates downward pore-water flow) fit measured sulfate profiles reasonably well. Note, to generate the modeled sulfate profiles, again we use either 15.5 cm (condition 1) or 100 cm (conditions 2 and 3) and zero sulfate as the lower boundary conditions (Dirichlet). Neither of the Dirichlet conditions (3–4) can be used in simulating DIC and ammonium profiles because there is no information available regarding deep DIC and ammonium concentrations in the sulfate free brine. However, using the two optimal *V* values obtained using the Dirichlet condition (1), pore-water DIC and ammonium profiles can also be largely explained as a result of conservative mixing. It is worth noting that the steady-state model we employed here only represents a simplified view of complex sediment systems associated with active brine activities, such that possible horizontal flow and non-steady-state conditions are not considered (which could be related to the irregularity in the ammonium profile at GB425). This simple advection–diffusion model clearly demonstrates that the upper 17 cm of the sediments at both sites are advection-dominated (e.g., using Cl^- as an example, advection accounts for 80% and 87% of the total fluxes at GB425 and GC233, respectively), and molecular diffusion (and perhaps reaction) plays a less important role in controlling pore-water solute distributions (Fig. 3).

Both upward and downward pore-water flow in cold seeps and seep-related sediments has been documented in the literature (Lapham et al., 2008; Ruppel et al., 2005; Solomon et al., 2008; Torres et al., 2002; Tryon et al., 2002). Upward flow in GC233 is probably caused by sediment compaction and geopressure/geothermal gradients (Joye et al., 2005). In addition, the close distance (<5 m) from our sampled GC233 site to the brine lake likely also contributes to the upward flow regime. Conversely, brine venting and gas discharge are both stronger in the GB425 mud volcano than those in the GC233 brine pool (Joye et al., 2005). Therefore, fluid discharge may have created a negative pressure gradient in its surrounding sediments which favors a density driven-convection (e.g., Solomon et al., 2008). This mechanism then allows downward seawater intrusion into the surrounding area of the mud volcano. This downward flow is consistent with both observed flow at a GB425 site (Ruppel et al., 2005) and a modeled flow scenario using a hypothetical salt dome (Ranganathan and Hanor, 1988).

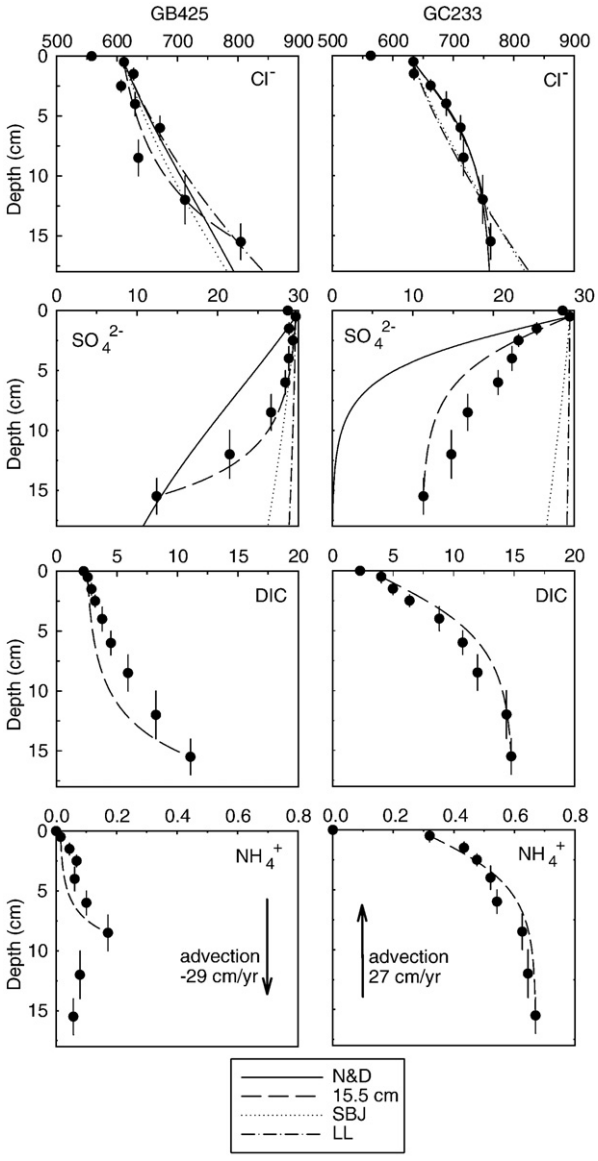

Fig. 3. Advection model fit to pore-water chloride, sulfate, DIC, and ammonium profiles. Four different types of boundary conditions are considered in the model (see Table 3 and text for details). The solid lines in the top two panels represent best model fit using the Neumann and Dirichlet (N&D) boundary conditions (i.e., measured chloride concentration at 0.5 cm and $dC/dx = 0$ at $x = \infty$). The dashed, dotted and dotted–dash lines represent model fits using the three Dirichlet boundary conditions as outlined in Table 3. The fits to the DIC and ammonium profiles were calculated using the advection rate obtained from the Dirichlet boundary condition (1). Note that the GB425 ammonium profile was only fit within the upper 10 cm sediments (see text for details). All concentration units are millimolar.

Interestingly, whether benthic organism (microbial mats and macrofauna) are in significant presence (i.e., forming visible mat) in seep-related environments appears to coincide with the direction of pore-water flow, or specifically, the presence of upward flow. The lack of visible microbial mats and benthic macrofauna at GB425 is probably caused by bottom seawater intrusion into the sediments or the lack of upward flow, since bottom water lacks dissolved constituents needed by chemosynthetic organisms. On the contrary, abundant microbial mats at our GC233 site and numerous mussels in surrounding area are probably caused by upward pore-water advection that brings up chemical energy (e.g., sulfide) which then facilitates chemosynthesis.

Table 3
Pore-water diffusion–advection model results.

	Model conditions[a]	V (cm yr^{-1})[b]	v_0 (cm yr^{-1})[c]	C_∞ (mM)[d]
GB425	1	6	6	1059
	2	−29	−30	–
	3	0	0	–
	4	2	2	–
GC233	1	27	31	765
	2	27	31	–
	3	−1	−1	–
	4	−4	−5	–

[a] Details of model condition, (1) Neumann and Dirichlet boundary conditions, $dC/dx = 0$ at $x = \infty$; and measured [Cl^-] at 0.5 cm; (2) Dirichlet boundary conditions, measured boundary [Cl^-] at 0.5 and 15.5 cm; (3) Dirichlet boundary conditions, measured [Cl^-] at 0.5 cm and brine [Cl^-] from Joye et al. (2005) with a modeled depth interval 100 cm; (4) Dirichlet boundary conditions, measured [Cl^-] at 0.5 cm and brine [Cl^-] from Lapham et al. (2008) with a modeled depth interval of 100 cm.
[b] Negative values indicate net downward pore-water advection.
[c] $v_0 = V/\varphi_0$, pore-water advection rate at sediment–water interface.
[d] Hypothetical chloride concentrations at infinite depth, these values were generated from the pore-water chloride profile modeling based on the model condition (1) only.

To determine whether pore-water mixing occurs, Chanton et al. (1991, 1993) used a simple approach by examining the relationships between pore-water solute concentrations and chloride concentration. Moreover, in their study near constant sulfate $\delta^{34}S$ with decreasing sulfate concentration along depth also reinforces the fact that sulfate reduction is not appreciable since advection caused sulfate removal is much faster. Similar plots of sulfate, DIC, and ammonium vs. chloride in this study also indicate that physical mixing dominates pore-water solute distributions in both sediments (Fig. 4), at least within our sampled depth interval (see Section 4.2 for the discussion of a subsurface reaction front). Our limited sulfate concentration ranges (lowest sulfate concentrations were 11–12 mM) prevent us from drawing a conclusion about the underlying brine-water chloride concentrations based on the linear extrapolations of SO_4^{2-} and Cl^- regression curve to zero sulfate, while Chanton et al. (1991, 1993) observed a complete depletion of sulfate so that such prediction was feasible.

4.2. Subsurface reaction front

Dissolution of salt deposits by buried sediment pore water leads to formation of brine water (Aharon et al., 1992). If no reaction that leads to alteration of pore-water DIC concentration occurs, a constant DIC concentration would be expected along the depth range of seawater and brine mixing. On the other hand, our pore-water model suggests that conservative mixing dominates the upper 17 cm sediments with conspicuous downcore pore-water DIC increase. Therefore, DIC increases in this mixing depth imply that there is a deeper DIC source that contributes to the pore-water DIC pool in the core depths. Taken together, it is likely that there is a subsurface reaction zone where sulfate oxidizes ascending organic matter, and the latter comes along with the efflux of brine (Fig. 5).

The subsurface reaction front is consistent with the well-known sulfate–methane interface (SMI) or sulfate–methane transition zone (SMTZ) widely observed in marine sediments, where methane is sourced from either upward migration of petroleum gases or methanogenesis at depth (Borowski et al., 1996; Borowski et al., 1999; Castellini et al., 2006; Iversen and Jorgensen, 1985; Kastner et al., 2008; Snyder et al., 2007; Ussler and Paull, 2008, and references therein). Oxidation of organic carbon in sedimentary environments, regardless of its source (i.e., planktonic or fossil carbon), leads to ^{13}C depletion in the pore-water DIC pool (e.g., McCorkle et al., 1985).

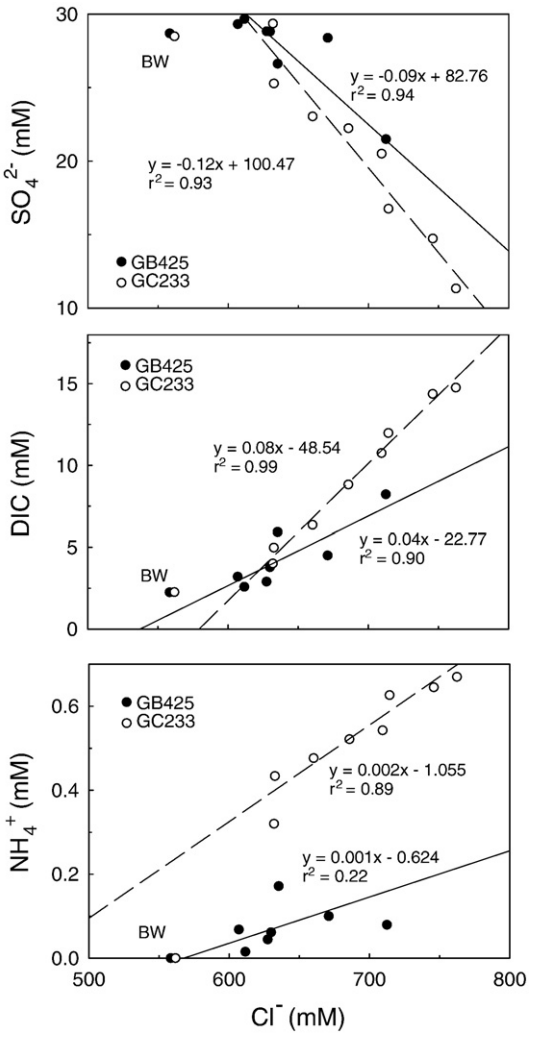

Fig. 4. The linear plots of pore-water sulfate, DIC, and ammonium vs. chloride. Note for GB425, only the upper 10 cm of pore-water data ($N = 6$) were used to generate the regression.

4.3. Pore-water $\delta^{13}C_{DIC}$ and possible carbon sources

Regressions of pore-water $\delta^{13}C \times DIC$ vs. DIC in sediment cores ranging from a few centimeters to tens of meters, from both seep

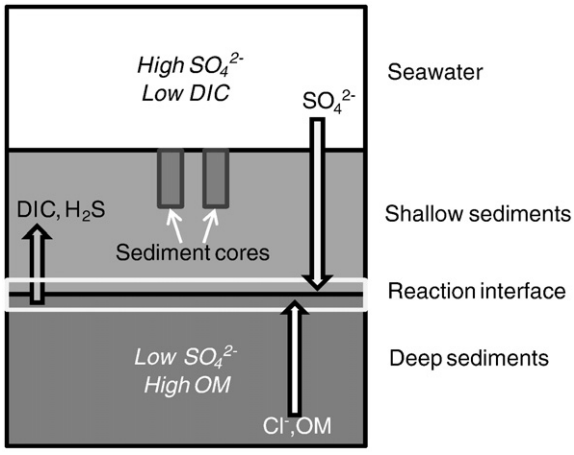

Fig. 5. Schematic illustration of pore-water transport-reaction zonation in GB425 and GC233 sediments. Note the relative positions of our sampled sediment cores to the deep reaction front.

(with or without brine influence) and common marine sediments, often times produce good linear relationships thus provide definitive $\delta^{13}C_{added}$ values in observed depth intervals (Fig. 6). Note in seep-associated sediments, good linear relationship is often observed in depths above the SMI (e.g., Borowski et al., 2000; Ussler and Paull, 2008). Using the calculated $\delta^{13}C_{added}$, one can use endmember carbon isotopic values to estimate contributions of different reactants to pore-water DIC pool. For example, if we assume two types of organic carbon in the Blake Ridge, gas-hydrate influenced sediments (Borowski et al., 2000), i.e., sedimentary organic carbon (or SOC, $\delta^{13}C = -21‰$) and methane ($\delta^{13}C = -101‰$), we can use a mass balance equation and calculate that methane oxidation contributes to ~35% of the added DIC to pore-water DIC pool over the entire depth range above the SMI (note the authors calculated methane oxidation contribute ~24% to DIC pool at the SMI only). Similarly, since the most negative $\delta^{13}C$ value of methane observed in the Mississippi Canyon methane-rich sediments is −89.5‰ (Ussler and Paull, 2008), if we take measured SOC $\delta^{13}C$ values that have a range between −23‰ and −28‰, methane oxidation would contribute 82–83% of the added DIC to pore-water DIC pool.

Previously reported $\delta^{13}C$ values of methane collected from brines at GB425 and GC233 are in the range of −60 to −64‰, and methane accounts for greater than 94% of the short-chain (C1–C5) hydrocarbon pool in these locations (Joye et al., 2005; Joye et al., 2009). It appears that methane is the major carbon source to brine-water DIC through anaerobic oxidation of methane (AOM), because $\delta^{13}C_{added}$ values at both stations (GB425, $-53.4 \pm 4.1‰$; GC233, $-58.6 \pm 2.1‰$) are close to the observed methane $\delta^{13}C$ values. Furthermore, if fractionation occurs, using a fractionation factor of 1.0088 (Alperin et al., 1988; although it ranges between 1.005 and 1.030, see Ussler and Paull, 2008), the estimated $\delta^{13}C$ of the remineralized methane would be ~−45‰ and ~−50‰ in GB425 and GC233, respectively. Either way, the $\delta^{13}C_{added}$ values are in general agreement with $\delta^{13}C$ values (−40 to −60‰) of a mixture of biogenic and thermogenic methane observed in the GOM seep environments (Formolo et al., 2004; Sassen et al., 1999; Sassen et al., 2003; Sassen et al., 2004).

Based on DIC isotopes, it appears that DIC production is linked to AOM. However, a series of recent studies contend that sulfate reduction rates far exceed those of AOM in GOM seep sediments (Joye et al., 2004; Joye et al., 2009; Orcutt et al., 2005). In these studies, high concentrations of non-methane organic compounds (e.g., longer-chained hydrocarbon, fatty acids) are found in addition to methane. First, venting gas can have methane $\delta^{13}C$ values as low as −90‰ (Joye et al., in press; Orcutt et al., 2005). Second, for the non-methane organic carbon, $\delta^{13}C$ values of both sedimentary particulate organic carbon (POC) and dissolved organic carbon (DOC) can be as low as −25‰ (Joye et al., 2004) and −30‰ (mainly acetate, Joye et al., 2009), respectively. Similar low acetate $\delta^{13}C$ values (−46‰) were also observed in Cascadia Margin sediments where gas hydrates are abundant (Heuer et al., 2009). From a different perspective, studies of authigenic carbonate also suggest that oxidation of non-methane hydrocarbons is also occurring in GOM seep sediments, and these hydrocarbons have similar isotopic composition as that of POC (e.g., Formolo et al., 2004).

Taken together, since our calculated $\delta^{13}C_{added}$ values fall in the range of the diverse $\delta^{13}C$ values of these different organic carbon sources, using $\delta^{13}C$ of respiration end product (i.e., DIC) alone in this complex sedimentary environment is inadequate to discern the exact carbon sources that contribute to the pore-water DIC pool. It is possible that sediments at these two sites could be subject to the co-occurrence of both the oxidation of non-methane organic carbon and AOM (e.g., Orcutt et al., 2005) with the latter possibly being less important (Joye et al., 2004). Nevertheless, from a mass balance point of view, $\delta^{13}C_{added}$ values reflect the bulk isotopic compositions of DIC that is produced through reaction pathways that are based on different organic carbon substrates (planktonic OC, long-chained hydrocarbon, and methane). To construct a mass balance for the added DIC here, first we take non-methane organic carbon $\delta^{13}C$ value of −20 to −30‰ as the heavy organic carbon endmember, the upper bound (−20‰) represents the $\delta^{13}C$ of POC produced at subtropical sea surface (Eadie and Jeffrey, 1973) and the lower bound (−30‰) represents non-methane hydrocarbons (Formolo et al., 2004), which also incorporates the $\delta^{13}C$ of DOC (Joye et al., in press). For the light organic carbon endmember, we take −60 to −90‰ as the end-member $\delta^{13}C$ values, both are measured methane $\delta^{13}C$ values (Joye et al., in press; Joye et al., 2005). Using the same mass balance discussed above, calculated light carbon contributions to DIC pool at these two sites are 48–78% and 55–95%, respectively. Clearly, this light carbon source(s) contributes no less than 50% to the overall sedimentary organic carbon remineralization in these brine-charged sediments. If AOM is not the dominant reaction pathway (Joye et al., in press; Joye et al., 2009), then fast production of this light carbon may be necessary to sustain high anaerobic oxidation (or sulfate reduction) rates. Future studies that integrate compound-specific, kinetic, and biological data (e.g., Heuer et al., 2009; Joye et al., 2009) in longer sediment cores (rather than the short push cores we used here) are

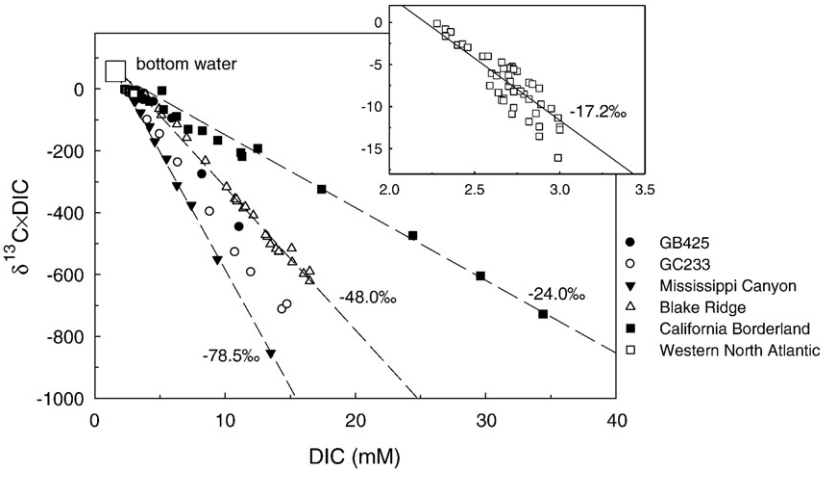

Fig. 6. Linear regression of $\delta^{13}C \times$ DIC vs. DIC in sediment pore waters from the literature. Data from both the Mississippi Canyon (Ussler and Paull, 2008) and Blake Ridge gas hydrate sediments (Borowski et al., 2000) are obtained at above the SMI depths (3 m and 20 m, respectively). Values shown in the figure are regressed $\delta^{13}C_{added}$ results. The insert is a blowup view of the Western North Atlantic sediment pore-water data (McCorkle and Emerson, 1988). Data from Blake Ridge, California Borderland (Presley and Kaplan, 1968), and Western North Atlantic are from multiple cores. Note that the Mississippi Canyon sediments contain methane that is of both biogenic and thermogenic origin, the Blake Ridge sediments have biogenic methane, and both the California Borderland and Western North Atlantic sediments are non-methanogenic.

necessary in elucidating problems of carbon sources and reaction pathways in these brine-influenced sediments.

5. Summary

Using a pore-water diffusion–advection model, we found that the upper 17 cm sediments of these two brine-charged sites are mainly controlled by pore-water advection. Furthermore, we found that a downward and an upward pore-water flow are present in GB425 and GC233, respectively, probably caused by nearby brine-seep activities. Evidence also points to a subsurface reaction front where sulfate reduction coupled with organic carbon oxidation is occurring. Subsequent conservative mixing between this DIC-laden yet sulfate depleted pore water with overlying bottom seawater dominates pore-water solute distributions in the upper 17 cm sediments.

Using stable isotope techniques, we determined that the $\delta^{13}C$ values of the oxidizing organic carbon in both sediments are in the range of a thermogenic and biogenic methane mixture (−40 to −60‰) found in the Gulf of Mexico. However, the stable carbon isotope composition of DIC alone appears unable to pinpoint the exact carbon form that is being remineralized in these complex systems. Future studies that incorporate detailed organic carbon, kinetic, and pore-water geochemical studies will be useful in determining organic matter remineralization pathways in these complex yet fascinating sediments.

Acknowledgements

Funding for this study was provided by the National Science Foundation and the National Undersea Research Program to the Shelf Slope Experimental Taphonomy Initiative (SSETI). We thank the shipboard scientific party and the captain and crew of the *R/V Seaward Johnson* and *Johnson Sea Link* for their help with sample collections. We thank D. Winter and D. Harris at UC Davis for their help with stable isotope measurements. Special thanks are also extended to G. Han for her help with pore-water analyses; Z. Huang and F. Wang for their assistance with sediment core processing; K. Parsons-Hubbard and E. Powell for their logistic support; S. Joye and C. Meile for the stimulating discussions related to this work; S. Joye and D. Burdige for offering insightful thoughts on an early draft of this work. Finally, W. Borowski, J. Trefry, and an anonymous reviewer all provided critical comments that improved this manuscript significantly.

References

Aharon, P., Roberts, H.H., Snelling, R.D., 1992. Submarine venting of brines in the deep Gulf of Mexico: observations and geochemistry. Geology 20, 483–486.
Alperin, M.J., Reeburgh, W.S., Whiticar, M.J., 1988. Carbon and hydrogen isotope fractionation resulting from anaerobic methane oxidation. Glob. Biogeochem. Cycles 2, 279–288.
Arvidson, R.S., Morse, J.W., Joye, S.B., 2004. The sulfur biogeochemistry of chemosynthetic cold seep communities, Gulf of Mexico, USA. Mar. Chem. 87, 97–119.
Berner, R.A., 1980. Early diagenesis - A Theoretical Approach. Princeton University Press, Princeton, N.J. 256 pp.
Borowski, W.S., Paull, C.K., Ussler III, W., 1996. Marine pore-water sulfate profiles indicate in situ methane flux from underlying gas hydrate. Geology 24, 655–658.
Borowski, W.S., Paull, C.K., Ussler III, W., 1999. Global and local variations of interstitial sulfate gradients in deep-water, continental margin sediments: sensitivity to underlying methane and gas hydrates. Mar. Geol. 159, 131–154.
Borowski, W.S., Hoehler, T.M., Alperin, M.J., Rodriguez, N.M., Paull, C.K., 2000. Significance of anaerobic methane oxidation in methane-rich sediments overlying the Blake Ridge gas hydrates. In: Paull, C.K., Matsumoto, R., Wallace, P.J., Dillon, W.P. (Eds.), Proc. Ocean Drill. Program, Sci. Results, pp. 87–99.
Boudreau, B.P., 1997. Diagenetic Models and Their Implementation — Modelling Transport and Reactions in Auqatic Sediments. Springer. 414 pp.
Burdige, D.J., 2006. Geochemistry of Marine Sediments. Princeton University Press. 609 pp.
Cai, W.-J., Wang, Y., 1998. The chemistry, fluxes, and sources of carbon dioxide in the estuarine waters of the Satilla and Altamaha Rivers, Georgia. Limnol. Oceanogr. 43, 657–668.
Cai, W.-J., Chen, F., Powell, E.N., Walker, S.E., Parsons-Hubbard, K.M., Staff, G.M., Wang, Y., Ashton-Alcox, K.A., Callender, W.R., Brett, C.E., 2006. Preferential dissolution of carbonate shells driven by petroleum seep activity in the Gulf of Mexico. Earth Planet. Sci. Lett. 248, 212–228.
Castellini, D.G., Dickens, G.R., Snyder, G.T., Ruppel, C.D., 2006. Barium cycling in shallow sediment above active mud volcanoes in the Gulf of Mexico. Chem. Geol. 226, 1–30.
Chanton, J.P., Martens, C.S., Paull, C.K., 1991. Control of pore-water chemistry at the base of the Florida escarpment by processes within the platform. Nature 349, 229–231.
Chanton, J.P., Martens, C.S., Paull, C.K., Coston, J.A., 1993. Sulfur isotope and porewater geochemistry of Florida escarpment seep sediments. Geochim. Cosmochim. Acta 57, 1253–1266.
Cline, J.D., 1969. Spectrophotometric determination of hydrogen sulfide in natural waters. Limnol. Oceanogr. 14, 454–458.
Eadie, B.J., Jeffrey, L.M., 1973. $\delta^{13}C$ analyses of oceanic particulate organic matter. Mar. Chem. 1, 199–209.
Formolo, M.J., Lyons, T.W., Zhang, C., Kelley, C., Sassen, R., Horita, J., Cole, D.R., 2004. Quantifying carbon sources in the formation of authigenic carbonates at gas hydrate sites in the Gulf of Mexico. Chem. Geol. 205, 253–264.
Gieskes, J.M., Mahn, C., 2007. Halide systematics in interstitial waters of ocean drilling sediment cores. Appl. Geochem. 22, 515–533.
Grasshoff, K., Kremling, K., Ehrhardt, M., 1999. Methods of Seawater Analysis. Wiley-VCH. 600 pp.
Heuer, V.B., Pohlman, J.W., Torres, M.E., Elvert, M., Hinrichs, K.-U., 2009. The stable carbon isotope biogeochemistry of acetate and other dissolved carbon species in deep subseafloor sediments at the northern Cascadia Margin. Geochim. Cosmochim. Acta 73, 3323–3336.
Holzbecher, E., 2007. Environmental Modeling Using MATLAB®. Springer. 392 pp.
Hu, X., 2007. Seagrass Mediated Carbonate Dissolution and Early Diagenesis in Bahamas Bank Sediments. Ph. D. Dissertation, Old Dominion University, Norfolk, VA, 201 pp.
Hu, X., Burdige, D.J., 2007. Enriched stable carbon isotopes in the pore waters of carbonate sediments dominated by seagrasses: evidence for coupled carbonate dissolution and reprecipitation. Geochim. Cosmochim. Acta 71, 129–144.
Iversen, N., Jorgensen, B.B., 1985. Anaerobic methane oxidation rates at the sulfate–methane transition in marine sediments from Kattegat and Skagerrak (Denmark). Limnol. Oceanogr. 30, 944–955.
Joye, S.B., Boetius, A., Orcutt, B.N., Montoya, J.P., Schulz, H.N., Erickson, M.J., Lugo, S.K., 2004. The anaerobic oxidation of methane and sulfate reduction in sediments from Gulf of Mexico cold seeps. Chem. Geol. 205, 219–238.
Joye, S.B., MacDonald, I.R., Montoya, J.P., Peccini, M., 2005. Geophysical and geochemical signatures of Gulf of Mexico seafloor brines. Biogeosciences 2, 295–309.
Joye, S.B., Samarkin, V.A., Orcutt, B.N., MacDonald, I.R., Hinrichs, K.-U., Elvert, M., Teske, A.P., Lloyd, K.G., Lever, M.A., Montoya, J.P., Meile, C.D., 2009. Metabolic variability in seafloor brines revealed by carbon and sulphur dynamics. Nat. Geosci. advanced online publication, doi:10.1038/ngeo475.
Joye, S.B., Bowles, M.W., Samarkin, V.A., Hunter, K.S. and Niemann, H., in press. Biogeochemical signatures and microbial activity of different cold seep habitats along the Gulf of Mexico lower slope. Deep-Sea Res. II.
Kastner, M., Claypool, G., Robertson, G., 2008. Geochemical constraints on the origin of the pore fluids and gas hydrate distribution at Atwater Valley and Keathley Canyon, northern Gulf of Mexico. Mar. Pet. Geol. 25, 860–872.
Kvenvolden, K.A., 1988. Methane hydrate — a major reservoir of carbon in the shallow geosphere? Chem. Geol. 71, 41–51.
Lapham, L.L., Alperin, M., Chanton, J., Martens, C., 2008. Upward advection rates and methane fluxes, oxidation, and sources at two Gulf of Mexico brine seeps. Mar. Chem. 112, 65–71.
LaZerte, B., 1981. The relationship between total dissolved carbon dioxide and its stable carbon isotope ratio in aquatic sediments. Geochim. Cosmochim. Acta 45, 647–656.
MacDonald, I.R., Reilly II, J.F., Guinasso Jr., N.L., Brooks, J.M., Carney, R.S., Bryant, W.A., Bright, T.J., 1990. Chemosynthetic mussels at a brine-filled pockmark in the northern Gulf of Mexico. Science 248, 1096–1099.
Martin, W.R., McNichol, A.P., McCorkle, D.C., 2000. The radiocarbon age of calcite dissolving at the sea floor: estimates from pore water data. Geochim. Cosmochim. Acta 64, 1391–1404.
McCorkle, D.C., Emerson, S.R., 1988. The relationship between pore water carbon isotopic composition and bottom water oxygen concentration. Geochim. Cosmochim. Acta 52, 1169–1178.
McCorkle, D.C., Emerson, S.R., Quay, P.D., 1985. Stable carbon isotopes in marine porewaters. Earth Planet. Sci. Lett. 74, 13–26.
Milkov, A.V., 2004. Global estimates of hydrate-bound gas in marine sediments: how much is really out there? Earth-Sci. Rev. 66, 183–197.
Muramatsu, Y., Doi, T., Tomaru, H., Fehn, U., Takeuchi, R., Matsumoto, R., 2007. Halogen concentrations in pore waters and sediments of the Nankai Trough, Japan: implications for the origin of gas hydrates. Appl. Geochem. 22, 534–556.
Orcutt, B., Boetius, A., Elvert, M., Samarkin, V., Joye, S.B., 2005. Molecular biogeochemistry of sulfate reduction, methanogenesis and the anaerobic oxidation of methane at Gulf of Mexico cold seeps. Geochim. Cosmochim. Acta 69, 4267–4281.
Pai, S.-C., Tsau, Y.-J., Yang, T.-I., 2001. pH and buffering capacity problems involved in the determination of ammonia in saline water using the indophenol blue spectrophotometric method. Anal. Chim. Acta 434, 209–216.
Parsons, K.M., Powell, E.N., Brett, C.E., Walker, S., Raymond, A., Callender, R., Staff, G., 1997. Shelf and Slope Experimental Taphonomy Initiative (SSETI): Bahamas and Gulf of Mexico: Proc. 8th Intl. Coral Reef Symposium, vol. 2, pp. 1807–1812.
Presley, B.J., Kaplan, I.R., 1968. Changes in dissolved sulfate, calcium and carbonate from interstitial water of near-shore sediments. Geochim. Cosmochim. Acta 32, 1037–1048.
Ranganathan, V., Hanor, J.S., 1988. Density-driven groundwater flow near salt domes. Chem. Geol. 74, 173–188.
Reimers, C.E., Jahnke, R.A., Thomsen, L., 2000. In situ sampling in the benthic boudary layer. In: Boudreau, B.P., Jfrgensen, B.B. (Eds.), The Benthic Boundary Layer: Transport Processes and Biogeochemistry. Oxford University Press, pp. 245–268.

Reitz, A., Haeckel, M., Wallmann, K., Hensen, C., Heeschen, K., 2007. Origin of salt-enriched pore fluids in the northern Gulf of Mexico. Earth Planet. Sci. Lett. 259, 266–282.
Ruppel, C., Dickens, G.R., Castellini, D.G., Gilhooly, W., Lizarralde, D., 2005. Heat and salt inhibition of gas hydrate formation in the northern Gulf of Mexico. Geophys. Res. Lett. 32 L04605/1-L04605/4.
Sassen, R., Joye, S., Sweet, S.T., DeFreitas, D.A., Milkov, A.V., MacDonald, I.R., 1999. Thermogenic gas hydrates and hydrocarbon gases in complex chemosynthetic communities, Gulf of Mexico continental slope. Org. Geochem. 30, 485–497.
Sassen, R., Milkov, A.V., Ozgul, E., Roberts, H.H., Hunt, J.L., Beeunas, M.A., Chanton, J.P., DeFreitas, D.A., Sweet, S.T., 2003. Gas venting and subsurface charge in the Green Canyon area, Gulf of Mexico continental slope: evidence of a deep bacterial methane source? Org. Geochem. 34, 1455–1464.
Sassen, R., Roberts, H.H., Carney, R., Milkov, A.V., DeFreitas, D.A., Lanoil, B., Zhang, C., 2004. Free hydrocarbon gas, gas hydrate, and authigenic minerals in chemosynthetic communities of the northern Gulf of Mexico continental slope: relation to microbial processes. Chem. Geol. 205, 195–217.
Schijf, J., 2007. Alkali elements (Na, K, Rb) and alkaline earth elements (Mg, Ca, Sr, Ba) in the anoxic brine of Orca Basin, northern Gulf of Mexico. Chem. Geol. 243, 255–274.
Snyder, G.T., Hiruta, A., Matsumoto, R., Dickens, G.R., Tomaru, H., Takeuchi, R., Komatsubara, J., Ishida, Y., Yu, H., 2007. Pore water profiles and authigenic mineralization in shallow marine sediments above the methane-charged system on Umitaka Spur, Japan Sea. Deep-Sea Res. II 54, 1216–1239.
Solomon, E.A., Kastner, M., Jannasch, H., Robertson, G., Weinstein, Y., 2008. Dynamic fluid flow and chemical fluxes associated with a seafloor gas hydrate deposit on the northern Gulf of Mexico slope. Earth Planet. Sci. Lett. 270, 95–105.
Torres, M.E., McManus, J., Hammond, D.E., de Angelis, M.A., Heeschen, K.U., Colbert, S.L., Tryon, M.D., Brown, K.M., Suess, E., 2002. Fluid and chemical fluxes in and out of sediments hosting methane hydrate deposits on Hydrate Ridge, OR, I: hydrological provinces. Earth Planet. Sci. Lett. 201, 525–540.
Tryon, M.D., Brown, K.M., 2004. Fluid and chemical cycling at Bush Hill: implications for gas- and hydrate-rich environments. Geochem. Geophys. Geosyst. 5.
Tryon, M.D., Brown, K.M., Torres, M.E., 2002. Fluid and chemical flux in and out of sediments hosting methane hydrate deposits on Hydrate Ridge, OR, II: hydrological processes. Earth Planet. Sci. Lett. 201, 541–557.
Ussler III, W., Paull, C.K., 2008. Rates of anaerobic oxidation of methane and authigenic carbonate mineralization in methane-rich deep-sea sediments inferred from models and geochemical profiles. Earth Planet. Sci. Lett. 266, 271–287.
Yeager, K.M., Santschi, P.H., Rowe, G.T., 2004. Sediment accumulation and radionuclide inventories (239, 240Pu, 210Pb and 234Th) in the northern Gulf of Mexico, as influenced by organic matter and macrofaunal density. Mar. Chem. 91, 1–14.